Structural phase-dependent hole localization and transport in bismuth vanadate

Kyoung E. Kweon and Gyeong S. Hwang*
Department of Chemical Engineering, University of Texas at Austin, Austin, Texas 78712, USA
(Received 9 January 2013; published 9 May 2013)

We present theoretical evidence for the phase dependence of hole localization and transport in bismuth vanadate ($BiVO_4$). Our hybrid density-functional theory calculations predict that, in the tetragonal phase [tetragonal scheelite $BiVO_4$ (ts-$BiVO_4$)], an excess hole tends to localize around a BiO_8 polyhedron with strong lattice distortion, whereas, in the monoclinic phase [monoclinic scheelite $BiVO_4$ (ms-$BiVO_4$)], it spreads over many lattice sites. The phase-dependent behavior is likely related to the higher structural stability of ms-$BiVO_4$ than ts-$BiVO_4$, which may suppress hole-induced lattice distortions. Our study also demonstrates that the relatively weakly localized hole in ms-$BiVO_4$ undergoes faster diffusion compared to the case of ts-$BiVO_4$, irrespective of the fact that the degrees of localization and mobility vary depending on the choice of exchange-correlation functional. The mobility difference may provide an explanation for the enhanced photocatalytic activity of ms-$BiVO_4$ over ts-$BiVO_4$ for water oxidation, considering that the increased mobility would lead to an increase in the hole current to the catalyst surface.

DOI: 10.1103/PhysRevB.87.205202 PACS number(s): 71.15.Mb, 71.20.Nr, 61.50.−f

I. INTRODUCTION

Bismuth vanadate ($BiVO_4$) has recently been recognized as a promising visible-light photocatalyst for water splitting and pollutant decomposition.[1–9] $BiVO_4$ mainly exists in three different crystal phases, such as tetragonal zircon (tz-), tetragonal scheelite (ts-), and monoclinic scheelite (ms-);[10] among them, ms-$BiVO_4$ has been found to exhibit the highest photocatalytic activity under visible-light irradiation.[2,3] The lower activity of tz-$BiVO_4$ has been explained[2] by its relatively large band gap of 2.9 eV, but the underlying reason for the superior performance of ms-$BiVO_4$ over ts-$BiVO_4$ still remains ambiguous. Although ms-$BiVO_4$ and ts-$BiVO_4$ have similar band gaps (2.4 and 2.3 eV, respectively[2]), the monoclinic lattice distortion is well known to induce modifications of the valance-band (VB) electronic structure of ms-$BiVO_4$;[11–13] especially, it has been suggested that the increased overlap between the Bi 6s and the O 2p orbitals would lead to enhanced migration of photogenerated holes in ms-$BiVO_4$.[2,3] However, despite their importance in determining the photocatalytic performance, the creation and transport of excess holes in $BiVO_4$ have been poorly studied.

In oxide semiconductors, excess charge carriers (electrons and holes) often remain localized.[14,15] The charge localization is commonly accompanied by lattice distortions, which results in a so-called polaron; a small polaron localizes at the atomic scale, whereas, a large polaron spreads over many lattice sites. The extent of localization also strongly affects the mobility of charge carriers.[14–17] Density functional theory (DFT) is perhaps the most successful computational method for the study of semiconductor and oxide materials; however, in practice, the results rely on approximations for the exchange-correlation (xc) potential that accounts for the many-body electron-electron interaction. In particular, the microscopic description of localized charge states tends to strongly depend on the xc energy functional employed. The (semi)local functionals of conventional DFT may fail to predict charge localization due to their inherent self-interaction error (which erroneously favors charge delocalization).[18,19] The self-interaction effects can be effectively canceled by partial inclusion of nonlocal Hartree-Fock (HF) exchange;[18–20] the HF/DFT hybrid approach has been shown to be capable of predicting charge localization and transport in many metal oxide semiconductor.[21–26]

In this paper, we investigate the dependence of hole creation and transport on the structural phases of $BiVO_4$ using hybrid DFT calculations. We first look at how the choice of xc functional affects the prediction of the closely correlated monoclinic distortion and valence-band electronic structure modification and attempt to select an adequate hybrid xc functional for describing the creation and transport of excess holes. Then, we examine the polaronic nature of excess holes in both ts-$BiVO_4$ and ms-$BiVO_4$ with comparisons to nonpolaronic (completely delocalized) states. Finally, the hole mobility difference between ts-$BiVO_4$ and ms-$BiVO_4$ is evaluated with a discussion of the underlying mechanism. This paper may also shed some insight into why ms-$BiVO_4$ and ts-$BiVO_4$ exhibit a considerable difference in photocatalytic performance.

II. COMPUTATIONAL METHODS

We performed spin-polarized DFT calculations using the Vienna *ab initio* simulation package (VASP 5.2.2).[27] The projector augmented wave method with a plane-wave basis set was used to describe the interaction between ion cores and valence electrons.[28] The valence-electron configurations considered are as follows: $5d^{10}6s^26p^3$ for Bi, $3p^63d^34s^2$ for V, and $2s^22p^4$ for O.

We used the Perdew-Burke-Ernzerhof (PBE) xc functional[29] and replaced a portion of the PBE exchange with exact HF exchange to obtain a hybrid functional. For hybrid DFT, we employed the Heyd-Scuseria-Ernzerhof (HSE) screened approach[30] in which long-range HF is excluded; note that the HF exchange interaction decays slowly with distance, making the conventional hybridization problematic for solids.[31,32] That is, the exchange term is split into short-range (SR) and long-range (LR) parts, and a fraction of the SR HF exchange is only included. As such, the xc energy is given by

$$E_{\mathrm{xc}}^{\mathrm{HSE}} = \alpha E_x^{\mathrm{HF,SR}}(\mu) + (1-\alpha)E_x^{\mathrm{PBE,SR}}(\mu) + E_x^{\mathrm{PBE,LR}}(\mu) + E_c^{\mathrm{PBE}},$$

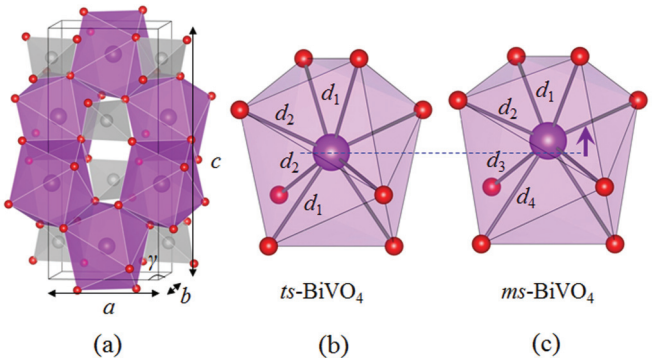

FIG. 1. (Color online) (a) Crystal structure representation of scheelite $BiVO_4$ with an indication of BiO_8 dodecahedra (in purple) and VO_4 tetrahedra (in gray) along with schematics of (b) symmetric BiO_8 dodecahedron in ts-$BiVO_4$ and (c) distorted BiO_8 dodecahedron in ms-$BiVO_4$. The arrow [in (c)] indicates Bi atom displacement along the c axis with respect to its corresponding position in ts-$BiVO_4$ (as indicated by the dotted line). There are two (d_1 and d_2) and four (d_1, d_2, d_3, and d_4) different kinds of Bi-O bond lengths in ts-$BiVO_4$ and ms-$BiVO_4$, respectively; the d values are listed in Table I. Purple, silver, and red balls represent Bi, V, and O atoms, respectively.

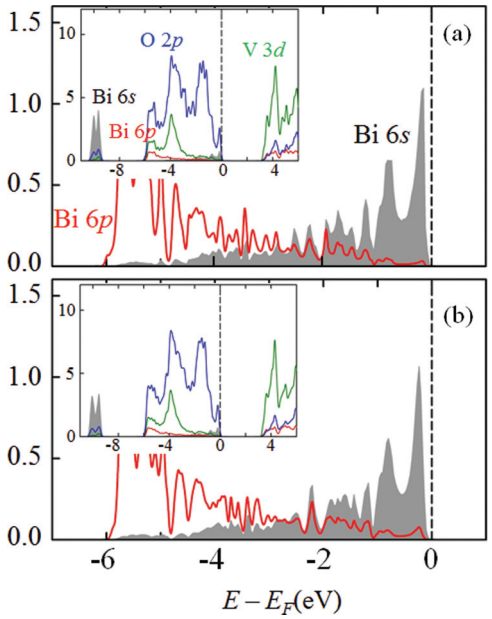

FIG. 2. (Color online) Electron density of states (DOS) projected onto Bi 6s (shaded in gray) and Bi 6p (red solid line) states in (a) ts-$BiVO_4$ and (b) ms-$BiVO_4$. In the inset, the blue and green solid lines indicate O 2p and V 3d states, respectively. The energy zero is set at the Fermi level (E_F), which is indicated by vertical dashed lines.

where the range-separation parameter μ determines the partition of the SR and LR components. In our paper, $\mu = 0.207$ Å^{-1} was used, which has already been demonstrated to be a reasonable compromise between accuracy and computational cost.[32]

For hole-doped $BiVO_4$, we used a supercell with 16 $BiVO_4$ formular units. A plane-wave cutoff energy of 400 eV and a $(1 \times 1 \times 1)$ k-point mesh were used for geometry optimization, and the k-point mesh size was increased up to a gamma-centered $(2 \times 2 \times 2)$ in refining the corresponding electronic structure. All atoms were fully relaxed using a conjugate gradient method until the residual forces on constituent atoms became smaller than 0.02 eV/Å. For the hole-doped system, one electron is removed from the neutral system, and the charge neutrality was ensured within the supercell by adding a compensating homogeneous background charge.

III. RESULTS AND DISCUSSION

A. Neutral $BiVO_4$

As illustrated in Fig. 1(a), the scheelite-type $BiVO_4$ structure consists of isolated VO_4 tetrahedra (in gray) that are corner connected by BiO_8 dodecahedra (in purple). $BiVO_4$ has been found to exist in the monoclinic scheelite phase at ambient temperature and pressure, and undergoes monoclinic-to-tetragonal phase transition under compression (around 1.5 GPa or 255 °C).[33,34] In ts-$BiVO_4$, Bi^{3+} cations are located at the centrosymmetric sites of BiO_8 polyhedra, whereas, the ms-$BiVO_4$ structure exhibits a distorted BiO_8 dodecahedron due to the Bi^{3+} off-centering [see Figs. 1(b) and 1(c)].

As presented in Fig. 2, analysis of the orbital-decomposed electron density of states (DOS) reveals that the top of the VB in ts-$BiVO_4$ is mainly composed of Bi 6s and O 2p states [in (a)], whereas there is an additional contribution of Bi 6p states in ms-$BiVO_4$ [in (b)], as also seen in the previous study.[35] In ts-$BiVO_4$, the coupling between occupied Bi 6s and O 2p states causes bonding and antibonding states below the Fermi level. The Bi 6s-O 2p antibonding destabilization is reduced by additional mixing with unoccupied Bi 6p states through the monoclinic lattice distortion, which may, in turn, make the monoclinic phase energetically more favorable than the tetragonal phase at ambient conditions. The energetically favored monoclinic distortion could also be explained by the pseudo Jahn-Teller effect.[36]

The predicted structures of ts-$BiVO_4$ and ms-$BiVO_4$ and their relative stability tend to be rather sensitive to the choice of xc functional.[35] We find that an increased amount of HF exchange leads to enhancement of the antibonding interaction between Bi 6s and O 2p states; as a consequence, hybridization between Bi 6s-O 2p antibonding states and unoccupied Bi 6p states becomes more pronounced to reduce the antibonding interaction through the monoclinic lattice distortion.

As summarized in Table I, the PBE-HF25% functional yields a monoclinic structure in very close agreement with the experimentally determined structure. On the other hand, the monoclinic distortion tends to be overestimated with PBE-HF50%, and the pure PBE and PBE-HF10% functionals can hardly identify a distinct monoclinic configuration under ambient conditions.[35] Considering the strong correlation between the monoclinic distortion and the VB-state modification, we believe that the PBE-HF25% functional can be adequate for describing the creation and transport of excess holes (as they are affected by modification of the valence-band top edge). Therefore, here, we only report the results from the PBE-HF25% approach.

TABLE I. Calculated lattice parameters (a, b, and c) and Bi-O bond lengths (d_1–d_4) for ts-$BiVO_4$ and ms-$BiVO_4$, together with experimentally measured values from Ref. 33 for comparison; see Fig. 1 for the schematics of ts-$BiVO_4$ and ms-$BiVO_4$. The a, b, c, and d values are given in angstroms (Å) and the monoclinic distortion angle (γ) is in degrees (°).

	PBE-HF25%		Experiment (Ref. 33)	
	ts-$BiVO_4$	ms-$BiVO_4$	ts-$BiVO_4$	ms-$BiVO_4$
a	5.121	5.183	5.147	5.215
b	5.121	5.074	5.147	5.084
c	11.647	11.711	11.722	11.706
γ	90	90.36	90	90.39
d_1/d_2	2.481/2.431	2.378/2.384	2.499/2.453	2.314/2.349
d_3/d_4		2.485/2.619		2.533/2.676

B. Hole-doped $BiVO_4$

We considered both localized (polaronic) and completely delocalized (nonpolaronic) hole states in ts-$BiVO_4$ and ms-$BiVO_4$. Here, a hole was created by removing an electron from the highest occupied orbital; recall that the top of the valance band consists of the hybrid Bi 6s-O 2p state in ts-$BiVO_4$ and the hybrid orbital of Bi 6s, Bi 6p, and O 2p in ms-$BiVO_4$. To create a polaronic state, we initially applied a small perturbation around a selected BiO_8 polyhedron to break the lattice symmetry prior to structural relaxation; otherwise, a nonpolaronic state is mostly conceived.[21,24]

First, the polaronic and nonpolaronic states in ts-$BiVO_4$ were examined. For the localized model, the hole state turns out to lie about 0.6 eV above the top of the VB according to our DOS calculations presented in Fig. 3(a). Figure 3(a) also shows the isosurface of the band-decomposed charge density that clearly demonstrates hole localization on the selected BiO_8 dodecahedron. About 14% of the hole charge is predicted to reside on the Bi site, and 60% is on the surrounding eight O atoms; the rest of the charge spreads out beyond the BiO_8 region. As illustrated in Fig. 3(a), the hole self-trapping is accompanied by local lattice distortions to yield a highly distorted BiO_8 polyhedron, indicating the formation of a small polaron. Notice a significant decrease in the Bi-O bond lengths (2.34/2.44 Å on average) in comparison to the neutral case (2.43/2.48 Å); this is apparently attributed to the depletion of the Bi 6s-O 2p antibonding orbitals that form the VB.

For the delocalized model [Fig. 3(b)], the Fermi level is shifted below the top of the VB, indicating hole creation in the VB. The corresponding band-decomposed charge-density isosurface reveals that the hole spreads over entire Bi and O atoms; recall that the top part of the ts-$BiVO_4$ VB is mainly composed of Bi 6s and O 2p states. The nonpolaronic state with no local lattice distortion, as expected, has the almost same configuration as the neutral state of ts-$BiVO_4$.

Our PBE-HF25% calculation predicts the small polaronic state to be 0.14 eV more favorable than the nonpolaronic state, suggesting the possibility of small polaron formation in ts-$BiVO_4$. Although we are unable to find previous reports on hole-doped ts-$BiVO_4$ for comparison, an earlier hybrid DFT study provides theoretical evidence of polaronic hole trapping in $BaBiO_3$.[26] Like ts-$BiVO_4$, the top of the $BaBiO_3$ VB is made up mainly of an antibonding combination of Bi 6s and O 2p orbitals, and the hole charge is found to predominantly localize around a BiO_6 octahedron. It might also be worthy to note that the polaronic hole trapping mediated by sp-like states tends to be distinct from that in binary metal oxides, such as TiO_2, Al_2O_3, and HfO_2 where the hole charge mostly resides at a single O site.[21,22,37]

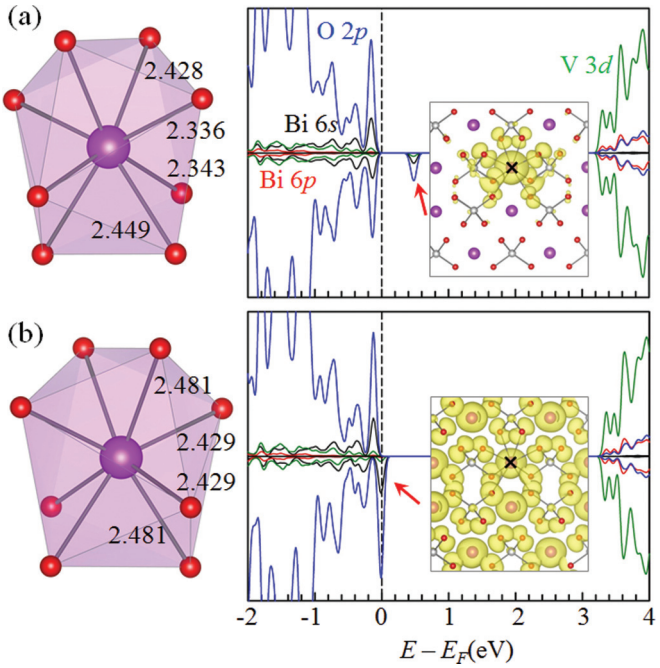

FIG. 3. (Color online) (Left panels) BiO_8 dodecahedron configurations and (right panels) orbital projected DOS for (a) polaronic and (b) nonpolaronic hole states in ts-$BiVO_4$. The insets (in right panels) show the band-decomposed charge densities of corresponding hole states (indicated by arrows) with isosurface values of (a) 0.010 $e/Å^3$ and (b) 0.002 $e/Å^3$; here, only the Bi-O bonds of selected BiO_8 dodecahedra are shown (and the corresponding bond lengths are indicated in Å in the left panels). In the DOS plots, the black, red, green, and blue solid lines indicate Bi 6s, Bi 6p, V 3d, and O 2p states, respectively. Purple, silver, and red balls represent Bi, V, and O atoms, respectively. The energy zero is set at the Fermi level (E_F), which is indicated by vertical dashed lines.

Next, we examined hole characteristics in ms-$BiVO_4$. As shown in Fig. 4(a), analysis of the electronic structure reveals that the polaronic hole state lies close to the VB edge. The hole charge is found to spread widely over two adjacent Bi-O layers with relatively weak lattice distortions around the hole-trapped region; only the shortest Bi-O bonds slightly decrease while the others remain nearly unchanged in comparison to the neural ms-$BiVO_4$ case. This may suggest that a large polaron would favorably form in ms-$BiVO_4$ rather than a small polaron.

For the delocalized model [Fig. 4(b)], the hole state exists at the top of the VB while being completely delocalized over Bi and O atoms. Notice the asymmetric charge distribution around Bi atoms indicating that Bi 6s orbitals are asymmetrically distributed in ms-$BiVO_4$; in contrast, in ts-$BiVO_4$ the Bi 6s lone pair remains spherically symmetric as demonstrated by the symmetric isosurface [see Fig. 3(b)].

In ms-$BiVO_4$, the large polaronic state turns out to be about 40 meV more favorable than the nonpolaronic state; the small

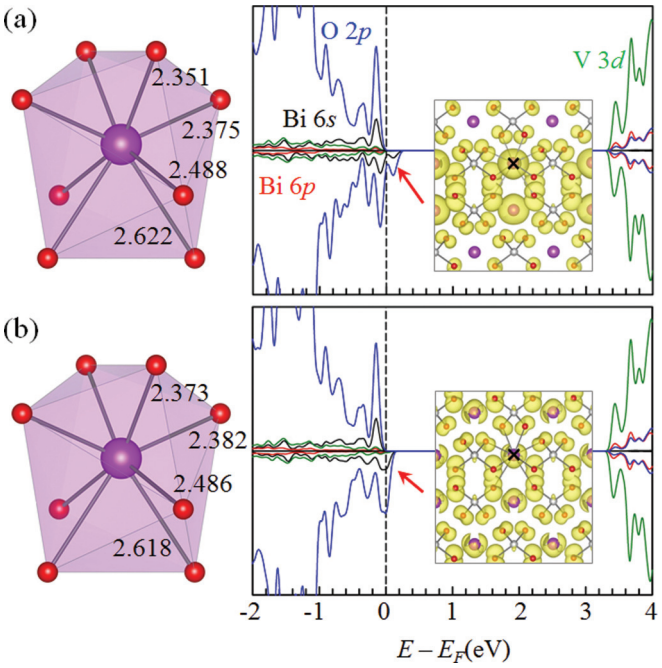

FIG. 4. (Color online) (Left panels) BiO_8 dodecahedron configurations and (right panels) orbital projected DOS for (a) polaronic and (b) nonpolaronic hole states in ms-$BiVO_4$. The insets (in right panels) show the band-decomposed charge densities of corresponding hole states (indicated by arrows) with an isosurface value of 0.002 $e/Å^3$; here, only the Bi-O bonds of selected BiO_8 dodecahedra are shown (and the corresponding bond lengths are indicated in Å in the left panels). In the DOS plots, the black, red, green, and blue solid lines indicate Bi 6s, Bi 6p, V 3d, and O 2p states, respectively. Purple, silver, and red balls represent Bi, V, and O atoms, respectively. The energy zero is set at the Fermi level (E_F), which is indicated by vertical dashed lines.

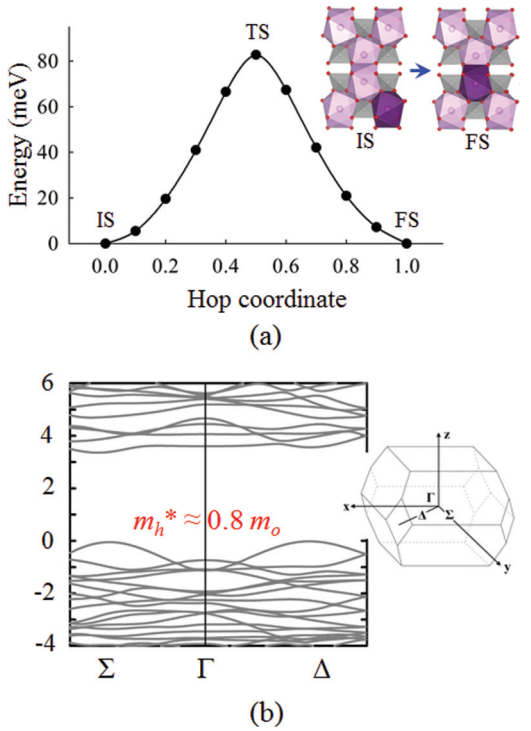

FIG. 5. (Color online) (a) Energy variation along the polaron migration path linearly interpolated between two minimum-energy configurations for ts-$BiVO_4$; the transition state (TS) occurs midway between the initial state (IS) and the final (FS) state. While the excess hole localizes around a BiO_8 polyhedron, the small-polaron positions in the initial and final states are colored in dark purple. (b) Band-structure diagram for ms-$BiVO_4$; the bands are plotted along the Σ and Δ directions as specified in the Brillouin zone.

energy difference can be expected considering their structural similarity. Although the degree of hole localization depends on the amount of HF exchange in the hybrid functional,[38] our study clearly demonstrates that ms-$BiVO_4$ has a relatively weak hole localization tendency than ts-$BiVO_4$. We suspect that this could be partially attributed to the greater structural stability of ms-$BiVO_4$ (*vide supra*), which may cause a higher energy cost for local polaronic lattice distortions, compared to the ts-$BiVO_4$ case; recall that the self-trapping of charge carriers occurs when the energy gain due to lattice polarization exceeds the strain energy caused by local lattice distortion.[22,23,39]

C. Phase dependence of hole transport

We attempted to estimate hole mobilities in ts-$BiVO_4$ and ms-$BiVO_4$ (which exhibit different degrees of hole localization as described above). Besides their relative sizes compared to the lattice constant, another important difference between small and large polarons is their transport behavior; migration of small polarons usually proceeds through thermally activated hopping, while large polarons tend to undergo band-like conduction.[14–16]

In ts-$BiVO_4$, we assume that hole transport follows the adiabatic small polaron hopping mechanism. As illustrated in Fig. 5(a), the hole migration can be described by a gradual change in the distorted lattice configuration between two adjacent polaronic configurations along the [101] direction; the intermediate configurations were linearly interpolated between the initial and the final configurations.[21,23–25,37] Since the initial and final states are identical, the transition state occurs midway between the two local minima. Our PBE-HF25% calculation predicts the energy difference between the initial and the transition states (= activation energy E_a) to be about 80 meV. Using Einstein's formula, the hole mobility (μ) can be approximated by $\mu = eD/k_BT = e(1-c)a^2\nu_0/k_BT\ \exp(-E_a/k_BT)$, where $(1-c)$ is the probability that a neighboring site is available for hopping, a is the hopping distance, and ν_0 is the longitudinal optical phonon frequency.[14,17] Taking $E_a = 80$ meV, $(1-c) \approx 1$, $a = 3.9$ Å, and $\nu_0 \approx 10^{13}$ Hz,[40] we obtained $\mu \approx 0.03$ cm^2 V^{-1} s^{-1} at room temperature, which is well below the theoretical upper limit of 1 cm^2 V^{-1} s^{-1} for the hopping mobility of small polarons.[14–17] This relatively high mobility may be attributed to the fact that a hole remains rather loosely localized in Bi 6s-O 2p hybridized orbitals. On the other hand, the mobility tends to be significantly reduced when a hole is strongly localized in a nonbonding 2p orbital of an O atom (e.g., $E_a = 0.40$ eV and $\mu \approx 10^{-6}$cm^2 V^{-1} s^{-1} in Ga_2O_3 at room temperature[22]).

In ms-$BiVO_4$, provided that the band-type conduction of large polarons is predominant, the hole mobility is given,[14,16] according to Drude's model, by $\mu = e\tau/m^*$, where τ is the scattering time and m^* is the effective hole mass. Here, we extracted m^* from the neutral primitive cell because of the high computational cost of obtaining the band structure of the hole-doped large supercell; this would be a valid approximation considering that the electronic structure of the large polaron state only slightly deviates from that of the nonpolaronic state (see Fig. 4). As demonstrated in Fig. 5(b), the band structure of neutral ms-$BiVO_4$ has a minimum direct gap in the Σ direction,[35] and the m^* value is estimated to be $\approx 0.8\ m_o$, while the top of the VB appears to be approximately parabolic. In many oxide materials, the scattering time τ is typically in the range of 10^{-12}–10^{-14} s at room temperature.[41,42] Hence, taking $\tau = 10^{-14}$ s and $m^* \approx 0.8\ m_o$, we obtained $\mu \approx 20\ cm^2\ V^{-1}\ s^{-1}$, which is about 3 orders of magnitude greater than $\mu \approx 0.03\ cm^2\ V^{-1}\ s^{-1}$ as predicted above for small polaron transport in ts-$BiVO_4$; this is consistent with the general trend that large polaron band-type conduction is much faster than small polaron hopping conduction.[14–16]

Here, we should admit that the predicted hole mobilities in $BiVO_4$ may vary to a certain degree depending on the amount of HF exchange in the hybrid functional. Nevertheless, our study clearly highlights that the tendency of relatively weak hole localization in ms-$BiVO_4$ will permit faster migration in comparison to the ts-$BiVO_4$ case. The increased hole mobility may, in turn, lead to an increase in the flux of photogenerated holes flowing to the $BiVO_4$ surface, thereby facilitating the hole-catalyzed oxidation of water. The phase-dependent hole mobility could provide an explanation why ms-$BiVO_4$ exhibits much higher photocatalytic performance than ts-$BiVO_4$.

IV. CONCLUSIONS

To summarize, we examined the creation and transport of an excess hole in tetragonal and monoclinic scheelite phases of $BiVO_4$ using hybrid DFT calculations. While predicted $BiVO_4$ properties vary depending on the choice of xc functional, our analysis suggests that the PBE-HF25% functional can give a reliable prediction of the tetragonal-to-monoclinic structural transition in comparison with existing experimental observations. The degree of the monoclinic distortion is found to be strongly correlated with the extent of hybridization between Bi $6s$-O $2p$ antibonding states and unoccupied Bi $6p$ states, and the valence-band electronic structure modification turns out to be sensitive to the amount of HF exchange in the hybrid functional. Given this, we thought the PBE-HF25% to be also adequate for describing the behavior of excess holes in $BiVO_4$, as it is largely influenced by modification of the valence-band top edge. According to our hybrid DFT calculations with the PBE-HF25%, the excess hole charge is predicted to localize around a BiO_8 polyhedron with significant lattice distortion in the tetragonal phase, while it spreads over many Bi and O lattice sites with an insignificant structural change in the monoclinic phase; the predicted small (large) polaronic state in ts-$BiVO_4$ (ms-$BiVO_4$) turns out to be 0.14 eV (0.04 eV) more favorable than the corresponding nonpolaronic state. Assuming the migration of small and large polarons occurs by thermally activated hopping and bandlike conduction, respectively, hole mobility in ms-$BiVO_4$ is predicted to be 2 to 3 orders of magnitude greater than that in ts-$BiVO_4$ at room temperature. Irrespective of the fact that the predicted mobility values tend to vary with different HF exchange fractions, our study unequivocally highlights that the relatively weak tendency of hole localization in ms-$BiVO_4$ compared to ts-$BiVO_4$ would lead to higher hole mobility. Although we cannot exclude the possible presence of other important factors, the phase-dependent hole mobility could help explain why ms-$BiVO_4$ exhibits much higher photocatalytic performance than ts-$BiVO_4$; note that the increased mobility may lead to an increase in the hole current to the catalyst surface, and thus, water oxidation can be facilitated.

ACKNOWLEDGMENTS

We would like to thank the Robert A. Welch Foundation (Grant No. F-1535) for financial support and the Texas Advanced Computing Center for use of their computing resources. Helpful discussions with A. J. Bard and W. A. Goddard III are also greatly acknowledged.

*Author to whom correspondence should be addressed: gshwang@che.utexas.edu

[1] A. Kudo, K. Omori, and H. Kato, J. Am. Chem. Soc. **121**, 11459 (1999).
[2] S. Tokunaga, H. Kato, and A. Kudo, Chem. Mater. **13**, 4624 (2001).
[3] J. Yu and A. Kudo, Adv. Funct. Mater. **16**, 2163 (2006).
[4] S. Kohtani, S. Makino, A. Kudo, K. Tokumura, Y. Ishigaki, T. Matsunaga, O. Nikaido, K. Hayakawa, and R. Nakagaki, Chem. Lett. **31**, 660 (2002).
[5] M. Long, W. Cai, J. Cai, B. Zhou, X. Chai, and Y. Wu, J. Phys. Chem. B **110**, 20211 (2006).
[6] K. Sayama, A. Nomura, T. Arai, T. Sugita, R. Abe, M. Yanagida, T. Oi, Y. Iwasaki, Y. Abe, and H. Sugihara, J. Phys. Chem. B **110**, 11352 (2006).
[7] H. Luo, A. H. Mueller, T. M. McCleskey, A. K. Burrell, E. Bauer, and Q. X. Jia, J. Phys. Chem. C **112**, 6099 (2008).
[8] H. Ye, J. Lee, J. S. Jang, and A. J. Bard, J. Phys. Chem. C **114**, 13322 (2010).
[9] H. S. Park, K. E. Kweon, H. Ye, E. Paek, G. S. Hwang, and A. J. Bard, J. Phys. Chem. C **115**, 17870 (2011).
[10] J. D. Bierlein and A. W. Sleight, Solid State Commun. **16**, 69 (1975).
[11] M. W. Stoltzfus, P. M. Woodward, R. Seshadri, J. Klepeis, and B. Bursten, Inorg. Chem. **46**, 3839 (2007).
[12] A. Walsh, Y. Yan, M. H. Huda, M. M. Al-Jassim, and S. H. Wei, Chem. Mater. **21**, 547 (2009).
[13] A. Walsh, D. J. Payne, R. G. Egdell, and G. W. Watson, Chem. Soc. Rev. **40**, 4455 (2011).
[14] A. J. Bosman and H. J. van Daal, Adv. Phys. **19**, 1 (1970).

[15]A. L. Shluger and A. M. Stoneham, J. Phys.: Condens. Matter **5**, 3049 (1993).
[16]D. Emin, Phys. Rev. B **48**, 13691 (1993).
[17]H. Böttger and V. V. Bryksin, *Hopping Conduction in Solids* (VCH, Deerfield Beach, FL, 1985).
[18]A. J. Cohen, P. Mori-Sánchez, and W. Yang, Science **321**, 792 (2008).
[19]P. Mori-Sánchez, A. J. Cohen, and W. Yang, Phys. Rev. Lett. **100**, 146401 (2008).
[20]M. Ernzerhof and G. E. Scuseria, J. Chem. Phys. **110**, 5029 (1999).
[21]D. Muñoz Ramo, A. L. Shluger, J. L. Gavartin, and G. Bersuker, Phys. Rev. Lett. **99**, 155504 (2007).
[22]J. B. Varley, A. Janotti, C. Franchini, and C. G. Van de Walle, Phys. Rev. B **85**, 081109 (2012).
[23]J. Kang, Y. S. Jung, S. H. Wei, and A. C. Dillon, Phys. Rev. B **85**, 035210 (2012).
[24]S. P. Ong, Y. Mo, and G. Ceder, Phys. Rev. B **85**, 081105 (2012).
[25]T. Maxisch, F. Zhou, and G. Ceder, Phys. Rev. B **73**, 104301 (2006).
[26]C. Franchini, G. Kresse, and R. Podloucky, Phys. Rev. Lett. **102**, 256402 (2009).
[27]G. Kresse and J. Furthmuller, *VASP: The Guide* (Vienna University of Technology, Vienna, Austria, 2001).
[28]P. E. Blöchl, Phys. Rev. B **50**, 17953 (1994).
[29]J. P. Perdew, K. Burke, and M. Ernzerhof, Phys. Rev. Lett. **77**, 3865 (1996).
[30]J. Heyd, G. E. Scuseria, and M. Ernzerhof, J. Chem. Phys. **118**, 8207 (2003).
[31]J. Paier, M. Marsman, K. Hummer, G. Kresse, I. C. Gerber, and J. G. Ángyán, J. Chem. Phys. **124**, 154709 (2006).
[32]L. Schimka, J. Harl, and G. Kresse, J. Chem. Phys. **134**, 024116 (2011).
[33]A. W. Sleight, H.-y. Chen, and A. Ferretti, Mater. Res. Bull. **14**, 1571 (1979).
[34]R. M. Hazen and J. W. E. Mariathasan, Science **216**, 991 (1982).
[35]K. E. Kweon and G. S. Hwang, Phys. Rev. B **86**, 165209 (2012).
[36]I. B. Bersuker, Chem. Rev. **113**, 1351 (2013); J. Phys.: Conf. Ser. **428**, 012028 (2013).
[37]N. A. Deskins and M. Dupuis, J. Phys. Chem. C **113**, 346 (2009).
[38]N. Sai, P. F. Barbara, and K. Leung, Phys. Rev. Lett. **106**, 226403 (2011).
[39]D. Emin, Phys. Today **35**, 34 (1982).
[40]R. L. Frost, D. A. Henry, M. L. Weier, and M. W. Martens, J. Raman Spectrosc. **37**, 722 (2006).
[41]T. Makino, A. Tsukazaki, A. Ohtomo, M. Kawasaki, and H. Koinuma, Jpn. J. Appl. Phys., Part 1 **45**, 6346 (2006).
[42]C.-W. Chen, Y.-C. Lin, C.-H. Chang, P. Yu, J.-M. Shieh, and C.-L. Pan, IEEE J. Quantum Electron. **46**, 1746 (2010).